ELSEVIER

Journal of Nuclear Materials 320 (2003) 194–208

journal of nuclear materials

www.elsevier.com/locate/jnucmat

Fractographic and microstructural characterization of irradiated 304 stainless steel intergranularly fractured in inert gas

T. Onchi [a,*], K. Dohi [a], N. Soneda [a], J.R. Cowan [b], R.J. Scowen [b], M.L. Castaño [c]

[a] *Central Research Institute of Electric Power Industry (CRIEPI), 2-11-1 Iwado Kita, Komae-shi, Tokyo 201-8511, Japan*
[b] *BNFL Research and Technology, Berkeley Centre, Berkeley, Gloucestershire, GL13 9PB, UK*
[c] *CIEMAT. Avda. Complutense, 22, Madrid 28040, Spain*

Received 26 July 2002; accepted 14 February 2003

Abstract

Fractographic and microstructural examinations were performed by scanning and transmission electron microscopy, respectively, and correlated, for the thermally sensitized 304 stainless steel (SS) irradiated to 1.2×10^{21} n/cm^2 ($E > 1$ MeV) in BWR condition and fractured intergranularly in 290 °C inert gas. Intergranular (IG) cracks were present in the specimen surface region and the fracture surface periphery. The fractography showed IG facets decorated with various patterns of linear features/steps. The microstructures of the surface region revealed linear features/deformation twinning near grain boundaries and microtwins at grain boundaries. The linear features identified on the [1 1 1] habit plane varied depending on deformation levels. The high number density of microtwins evidences a high local stress and strain concentration, which may nucleate and initiate at the impingement of deformation twins and grain boundaries. Therefore we conclude that a mechanism causing the IG cracking mechanically in non-aqueous environment is present in the highly irradiated austenitic SS.

PACS: 61.72.−y; 61.72.−Lk; 61.72.−Mm; 61.80.−x; 61.80.−HG; 62.20.Fe; 68.37.Lp

1. Introduction

Austenitic stainless steels (SSs) have been used as core component materials for light water reactors (LWRs). During long-term service the SSs suffer radiation damage in water environment, resulting in material degradation typified by irradiation assisted stress corrosion cracking (IASCC). It is acknowledged that the IASCC occurs in non-sensitized SSs when neutron fluence accumulated in the materials exceeds over the IASCC fluence thresholds. Our knowledge of IASCC has been gained mostly from the results of the slow-strain-rate-test (SSRT), which is performed to examine whether or not the irradiated SSs can fracture intergranularly in water environment. However, if a mechanism causing intergranular (IG) cracking in the irradiated SSs is present in non-aqueous environment, all the IG cracks generated in water environment cannot be regarded as being produced in an IASCC process, that is, some cracks may possibly be also in a mechanical IG cracking process. Therefore it is essential to study the cause and effect relation of plastic deformation behavior and IG fracture of the irradiated SSs in order to improve mechanistic understanding of the IASCC.

* Corresponding author. Tel.: +81-3 3480 2111; fax: +81-3 3480 7950.
E-mail address: tonchi@criepi.denken.or.jp (T. Onchi).

0022-3115/03/$ - see front matter
doi:10.1016/S0022-3115(03)00105-3

Historically the IG fracture phenomenon of the core component materials was recognized throughout the 1980s and termed as IASCC in BWR and then in PWR as well. Before that time, however, the plastic deformation and fracture of the irradiated SSs had been comprehensively studied. Based on a large quantity of data, Bloom [1] developed a schematic representation of the stress and temperature dependence of the fracture behavior of 304 SSs after irradiation to high fluences. He showed that at the LWR temperature regime of below 350 °C radiation induced dislocation loops are capable of changing plastic deformation mode to localized planar or channel deformation, which results in causing grain boundary fracture and also a specific type of ductile fracture along the deformation channel (the so-called channel fracture). The mechanistic insight into the change in fracture modes given by Bloom was that at higher temperatures where the grain boundary tends to be weaker than the matrix, grain boundary cracks may be initiated at the intersection of the localized deformation channel with the grain boundary, although the mechanism of crack initiation and stable growth is not certain.

Since the 1980s, concern and interest have been focused on studying the IASCC in water environment. In the course of the studies, nevertheless, attempts have been made to produce the IG cracks in non-aqueous environment by several workers, who performed the SSRT of the irradiated SSs in inert gas or in air at BWR and PWR temperatures. Although no IG fracture occurred in inert gas or in air for the solution annealed and the thermally sensitized 304 SSs irradiated and tested at BWR condition [2–5], the inert gas IG cracks were found for the cold worked 316 SSs irradiated and tested at PWR condition [6–8] and for the solution annealed 304 SS irradiated and tested at BWR condition [9]. In spite of the controversial reproducibility[10], however, it is a certain fact that IG cracking can occur without an aqueous environment. Thus it is essential to investigate mechanism of the IG cracking in inert gas for more general mechanistic understanding of IG cracking phenomena, inclusive of IASCC, in the irradiated austenitic SSs.

Recently we presented the IG cracking of a thermally sensitized 304 SS sample irradiated to 1.2×10^{21} n/cm^2 ($E > 1$ MeV) and examined by the SSRT in 290 °C inert gas [11,12]. We believe that the sample is useful for carefully investigating and identifying the real cause of the inert gas IG cracking. The objectives of this work are therefore to characterize a detailed fractographic and microstructural features of the IG cracked sample and to correlate them to each other to study the mechanism of the IG cracking. The neutron fluence of 1.2×10^{21} n/cm^2 to which the 304 SS was irradiated is approximately two times larger than the neutron fluence threshold of 5×10^{20} n/cm^2 for IASCC in BWR condition. Since the IG cracks were present in the surface region of the irradiated SS sample, an especial emphasis is placed on the TEM examination of the specimen surface layer.

2. Experimental

The 304 SS sample, irradiated to 1.2×10^{21} n/cm^2 ($E > 1$ MeV) at a BWR condition in test reactor and fractured intergranularly in 290 °C inert gas, were primarily used for this work. Those unirradiated and irradiated to 1.1×10^{20} n/cm^2 and fractured in ductile manner at the same conditions were also added to this work for comparison. The procedures of the specimen fabrication, the neutron irradiation and the SSRT in inert gas were outlined in the following.

An original 304 SS tube having an outer diameter of 10 mm and a thickness of 1 mm was machined and shaped into tensile specimens with a gauge length of 16 mm, a width of 3 mm and a thickness of 1 mm. The specimen has concave and convex surfaces. The chemical composition is shown in Table 1. The carbon content of the specimen is 0.05 wt%, which is classified as the high carbon SS. The specimens were solution annealed and then thermal sensitization heat-treated at 750 °C for 100 min. and subsequently at 500 °C for 24 h to provide a large chromium depletion at the grain boundary. A typical transmission electron micrograph of an unirradiated, thermally sensitized specimen is presented in Fig. 1, showing undeformed grain matrix and grain boundaries with and without carbide precipitates.

The neutron irradiation of the tensile specimens was performed to a higher neutron fluence of 1.2×10^{21} n/cm^2 ($E > 1$ MeV) in a simulated BWR water in Halden reactor, and to a lower fluence of 1.0×10^{20} n/cm^2 in 290 °C inert gas in JMTR. After the irradiation, the SSRT were carried out in 290 °C inert gas with an average strain rate of 3.5×10^{-7} s^{-1} (a cross head speed of 0.33 μm/min) at CIEMAT hot cell facilities. Mechanical properties of the unirradiated and irradiated specimens were determined from the chart recording during the SSRT. The fractured specimens were ultrasonically

Table 1
Chemical composition of the unirradiated specimen

Chemical element	C	Si	Mn	P	S	Ni	Cr	Co	Fe
wt%	0.05	0.61	0.88	0.022	0.014	9.4	18.6	0.002	Balance

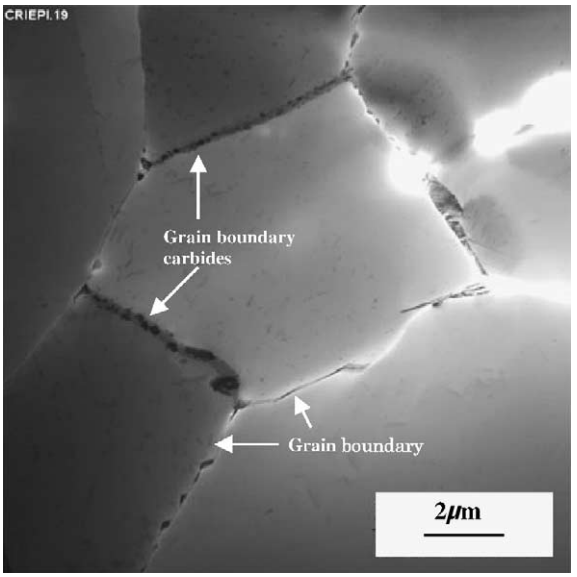

Fig. 1. A typical transmission electron micrograph of the unirradiated material.

cleaned. More detailed experimental procedures and test results were presented elsewhere [11,12].

Fractography and microscopy of the fractured specimen were conducted at BNFL Berkeley Center. Extensive observations of the concave and convex surfaces and the fracture surface were carried out in the fully shielded JEOL 6100 scanning electron microscope (SEM). After the SEM work, the sample was cut along the gauge length to obtain slices parallel to fracture face. A slice for microscopy was taken from the un-necked portion, where many IG cracks were present in the specimen surface region, at a position of 3.5 mm from the fracture face. The bottom side (concave surface) of the slice was ground until just flat, and then the upper side (convex surface) until the residual thickness was approximately 0.1 mm. The remaining slice of approximately 100 μm was electropolished in a solution of 5% perchloric acid in butoxyethanol, using a Tenupol-2 polishing unit operating at approximately 20 °C and a voltage of 30 V DC. The perforated slice was examined with a 300 kV Jeol 3010 transmission electron microscope (TEM). The other slices at several positions along the gauge section were also used for the microscopy of the central region of the specimen thickness.

3. Results

Table 2 lists mechanical properties and IG fracture ratio for the unirradiated and irradiated specimens used for the TEM microscopy. Yield and tensile stresses increase and uniform and total elongations decrease with increasing neutron fluence, which are consistent with the data from another series of the irradiated thermally sensitized 304 SSs [2].

3.1. SEM Fractography

3.1.1. Specimen surface

A concave surface appearance of the fractured specimen irradiated to 1.2×10^{21} n/cm^2 is presented in Fig. 2. The length of the necked portion is about 2.5 mm and the fracture face is located in the front edge of the necked portion. The fracture face appears having a typical mode of shear fracture. At a glance, there are numerous cracks over the concave surface of the gauge length, as seen in Fig. 2. Most of all the cracks on the concave surface lie in the transverse direction along the grain boundaries, indicating that the crack mouth was opened primarily by the axial tensile force. The appearance of the IG cracks is unchanged so much in the necked and un-necked portions, although those IG cracks are likely to have been formed one after another during straining until the necking in the SSRT. The observed IG cracks are roughly grouped into angular IG cracks and roundish IG cracks. Based on the specific appearances of the interior and exterior regions of the individual IG cracks, it is assumed that the angular cracks were formed in the lower level of plastic deformation whereas the roundish cracks are shaped in the higher level of deformation.

Table 2
Mechanical properties of the unirradiated and irradiated specimens used for the TEM microscopy

Neutron fluence (n/cm^2, $E > 1$ MeV)	Unirradiated (Sp. no. 30)	1.1×10^{20} (Sp. no. 2)	1.2×10^{21} (Sp. no. 36)
Mechanical properties			
Yield stress (MPa)	134	406	608
Maximum tensile stress (MPa)	504	608	656
Strain to maximum stress (%)	48	36	16
Strain to fracture (%)	51	40	18
Fractography			
IG fracture ratio (%IG)	0	0	7

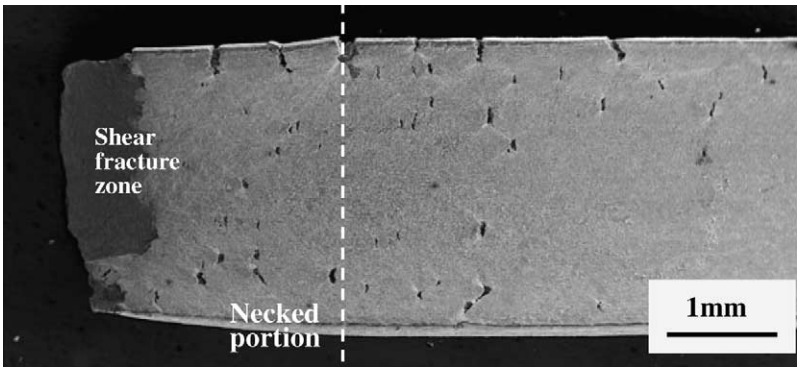

Fig. 2. A concave side appearance of the gauge section for the fractured specimen.

Fig. 3 shows an example of an angular IG crack. The IG crack is surrounded with brittle matrices (Fig. 3(a)). In the interior of the crack some grains have smooth IG facets with precipitates (Fig. 3(b)) and some have geometrical patterns of linear features/steps (Fig. 3(c)). The term, linear features, was provided specifically for this work because of less evidences of slip deformation in the highly irradiated 304 SS, although such patterns are generally named 'slip steps' in the IG facets by IASCC workers. There was no evidence of oxides in the interior surfaces of the IG crack, suggesting that the crack occurred during straining in inert gas, and neither during irradiation in water environment nor during long term wet storage after irradiation.

Fig. 4 presents an example of a roundish IG crack. The crack is surrounded with heavily deformed matrices (Fig. 4(a)). Most IG facets are designed with large angle grain boundary step (Fig. 4(b)) and some grains are also decorated densely with cross steps following linear features (Fig. 4(c)). These heavily crossed deformation steps indicate that the roundish cracks were formed in the high level of plastic deformation. There was no oxidation in the interior of the IG facets in any of the cracks.

A convex surface appearance of the necked and fractured portion is shown in Fig. 5, indicating a few large cracks, which are IG cracks in nature, and the presence of possible deformation banding lying at 45° to the gauge length. The presence of the thick oxide layer however prevented a detailed examination of these features. The possible deformation banding and the large cracks are likely linked together. No evidence of oxides on the interior IG cracks shows that the cracks were produced during the SSRT.

3.1.2. Fracture surface

A fracture surface of the intergranularly fractured specimen is presented in Fig. 6, consisting of the ductile microvoid coalescence (MVC) for the most part and the 7% IG fracture only in the surface periphery. A number of IG crack zones were present in the concave side edge and one in the convex side edge over the entire fracture surface. It should be noted that all the IG cracked zones were isolated to each other. The IG cracks extended approximately 100 μm into the sample bulk from the surface (an order of several grains). No oxidation of any IG facets was detected in the fracture surface.

3.2. TEM microscopy

General TEM microstructures of the irradiated, thermally sensitized 304 SS intergranularly fractured in inert gas contained radiation induced dislocation loops of a faulted (Frank) type, stacking faults, Cr carbides precipitates at grain boundaries and in the grain matrices, microtwins and linear features/deformation twins at or near the grain boundaries, in either of the specimen thickness center and the specimen surface layer. Specific microstructures in the region of specimen thickness center were characteristic of densely populated linear features/deformation twins, martensite formation at the intersection of deformation twins, austenite matrix regions and so on in the high deformation region. The absence of any IG cracks in the central region however prevented us from a direct correlation between the TEM microstructures and the IG cracking. Thus more efforts were made for examining the approximate 100 μm concave surface region at a location of 3.5 mm away from the fracture face.

3.2.1. Specimen surface region

Among grains available for the TEM examination within the TEM foil sample two different type of grains, labeled A and B, in high and low deformation levels, respectively, were selected and used to investigate microstructural features of the intergranularly cracked region. Fig. 7 shows general microstructures at a low magnification in grain A containing a grain boundary

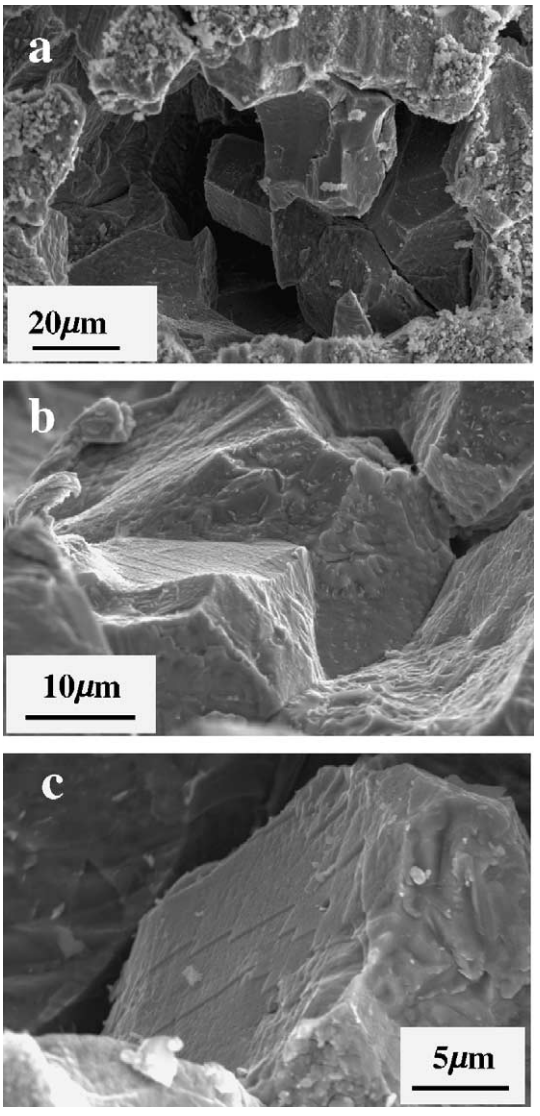

Fig. 3. An example of an angular IG crack (a). Some interior grains have rough IG facets (b), with patterns of linear features (c).

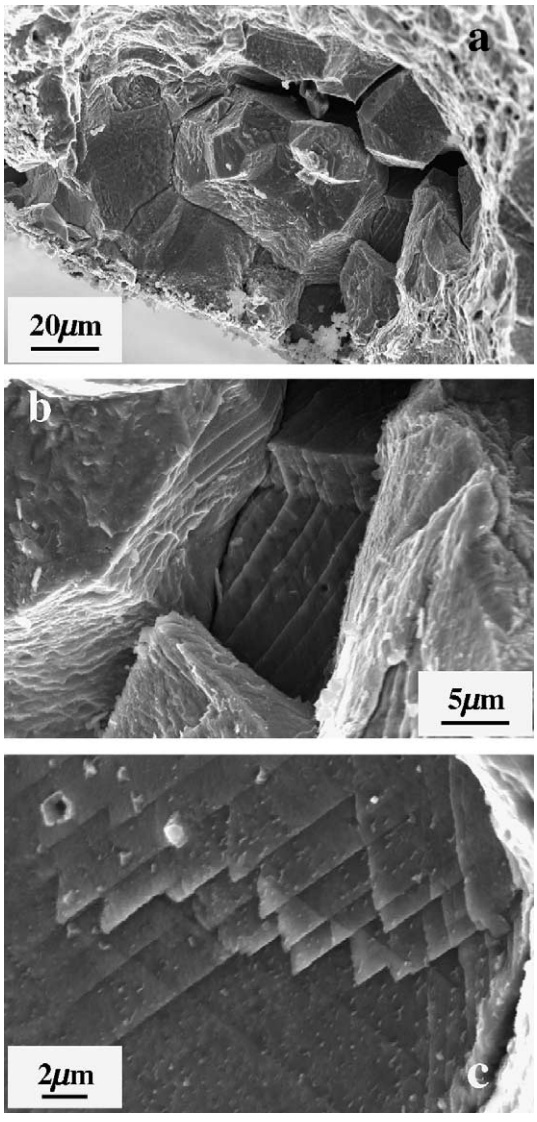

Fig. 4. An example of a roundish IG crack (a). Some interior grains have IG facets designed densely with large grain boundary steps (b) and with cross steps following linear features (c).

and a grain matrix decorated with linear features running across the entire grains with a background of high contrast.

Fig. 8 shows a higher magnification micrograph of the background contrast, revealing a large number of irradiation-induced dislocation loops throughout the microstructure. The selected area diffraction pattern (SADP) showed the loops to lie on the fcc [1 1 1] type planes. Examination of the loop population gave a mean diameter of 5 ± 2 nm (standard deviation) with a number density of 1.7×10^{22} m^{-3}. The loop size is well comparable to published data [10], with a number density slightly lower than that in the literature. The results of more detailed deformation microstructures in grain A and grain B, which are different in deformation levels, are described below.

3.2.1.1. Low deformation microstructure – Grain B. The general microstructure within grain B at low magnification shows the presence of a series of large linear features, which run approximately parallel to the grain boundary, extending across the entire grain. The structure of the linear feature away from the grain boundary is shown in Fig. 9 at high magnification. Imaged with electron beam direction $B = [1\,0\,1]$, the feature is made

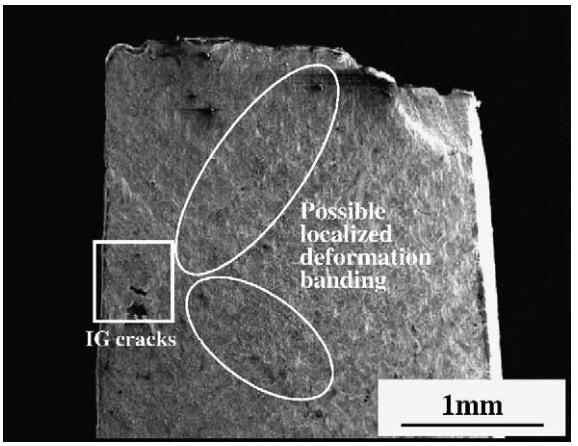

Fig. 5. A convex surface appearance of the necked and fractured portion indicating the presence of a few large cracks associated with possible deformation banding.

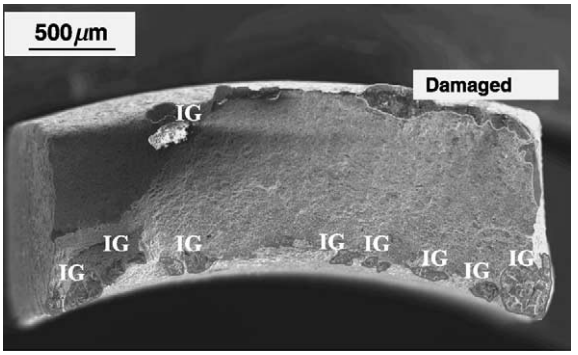

Fig. 6. Fracture surface exhibiting IG cracks in the periphery over the fracture surface.

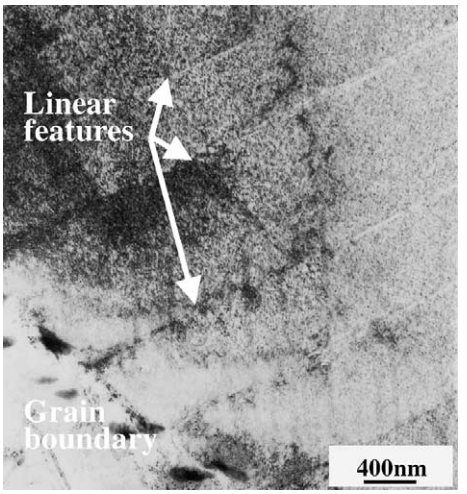

Fig. 7. General microstructures of the surface region at a low magnification consisting of grain boundary and grain matrix decorated with linear features within a background of high contrast.

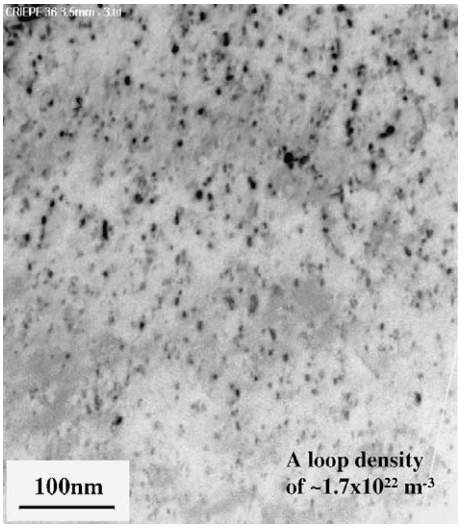

Fig. 8. A higher magnification microstructure of background contrast revealing a large number of irradiation induced loops.

up of dislocation tangles with small microtwin nuclei. The SADP of the region marked with a square shows a [1 0 1] matrix pattern, with streaking of the [2 0 2] type reflections (Fig. 9(a)), typical of the presence of thin twins or stacking faults. In a higher magnification image of the region marked with the square in Fig. 9(a), the linear feature is composed of dislocation tangles and very fine microtwins (arrow indicates about 20 nm long features, Fig. 9(b)).

Closer and parallel to the grain boundary of the same image with beam direction $B = [1\,0\,1]$ in grain B, other linear features appear as channels, clear from radiation produced loops, as observed in Fig. 10. These clear channels appear to be bounded at the channel walls by microtwin nuclei, which give rise to the slight streaking of the SADP (Fig. 10(a)). The channel wall in the area within the dashed square in Fig. 10(a) appear to contain extended microtwins nuclei (indicated by the arrows encircled, Fig. 10(b)).

Fig. 11 shows a linear feature adjacent to the grain boundary in grain B. The linear feature is observed corresponding to a fully developed deformation twin, because the SADP from the area marked by the square contains distinct extra spots (Fig. 11(a)), when viewed with beam direction $B = [1\,0\,1]$. This feature is also clear from irradiation loops. Unlike the channel in Fig. 10(a), the channel is bounded with fringes (Fig. 11(b)).

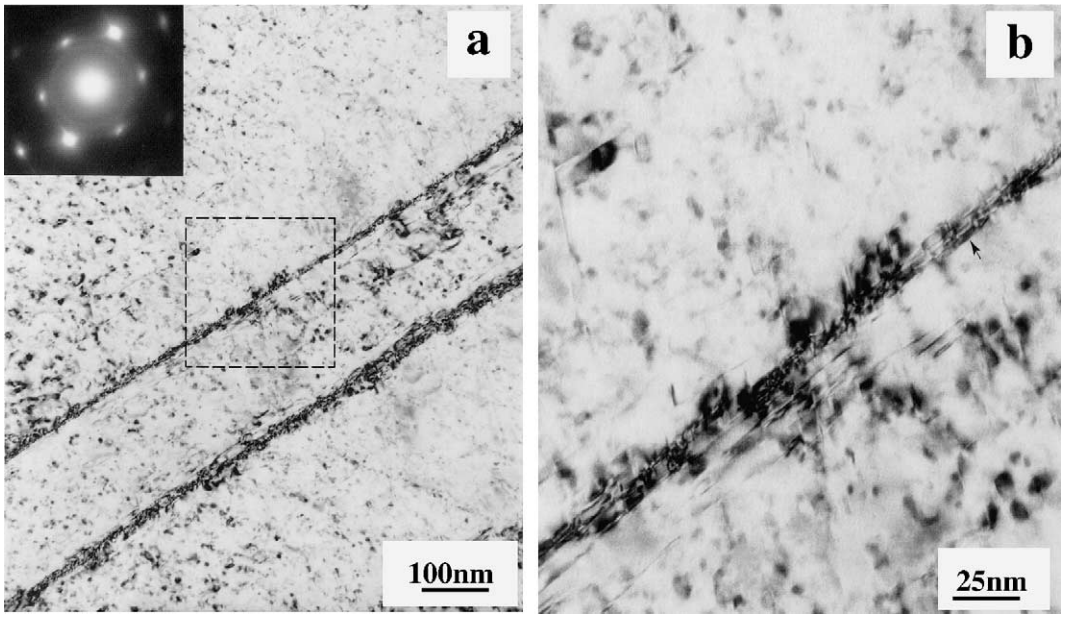

Fig. 9. A high magnification image of linear features away from the grain boundaries being made up of dislocation tangles with small microtwin nuclei (a). A higher magnification image of a linear feature in a region marked with a square in (a) being composed of dislocation tangles and very fine microtwins (b).

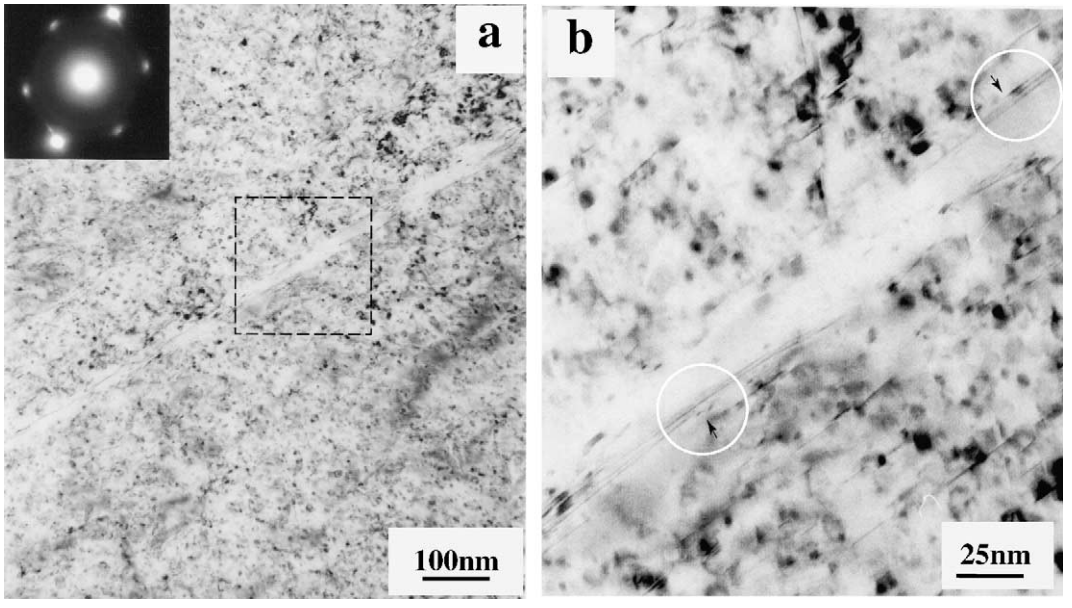

Fig. 10. The linear features closer parallel to the grain boundary appearing as channels bounded at the channel walls by microtwin nuclei (a). The microtwin nuclei in the channel walls is indicated by the encircled arrows (b).

3.2.1.2. High deformation microstructure – Grain A. Fig. 12 shows low and high magnification images of the [1 1 1] type planes near to the grain boundary in grain A. The low magnification image of a grain matrix and a grain boundary decorated with carbides contains a large number of linear features with a spacing of about 600 nm and also microtwins (Fig. 12(a)). Imaged with electron beam direction $B = [1\,1\,2]$, these linear features appear as channels, clear from loops. Close to the grain boundary, hands of microtwins lying on the [1 1 1] type

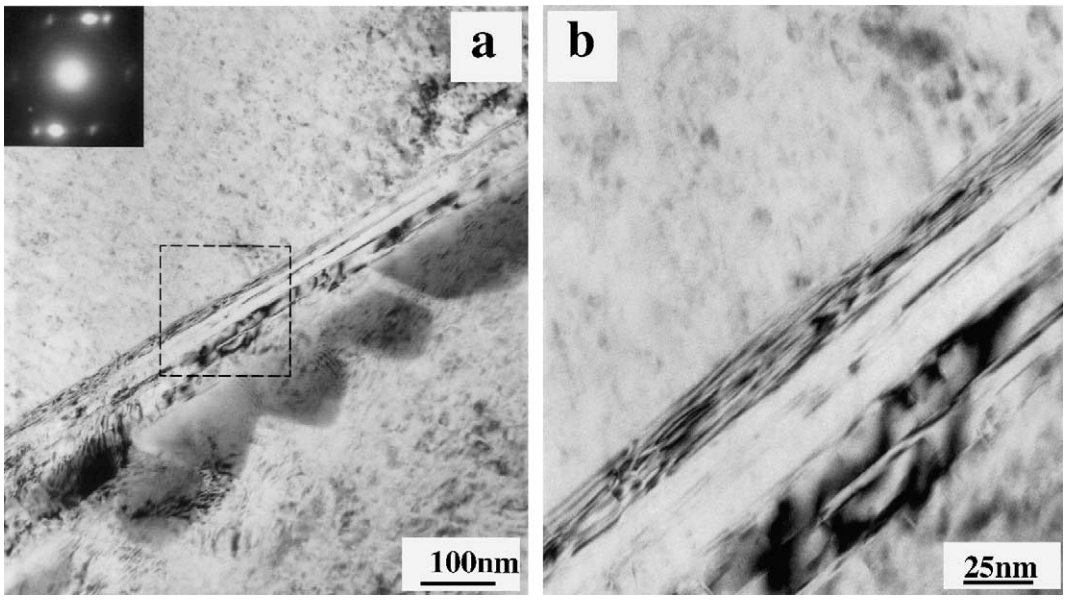

Fig. 11. The linear features adjacent to the grain boundary correspond to a fully developed deformation twins (a). The channel features from the area marked by the square in (a) was clear from loops and bounded by fringes (b).

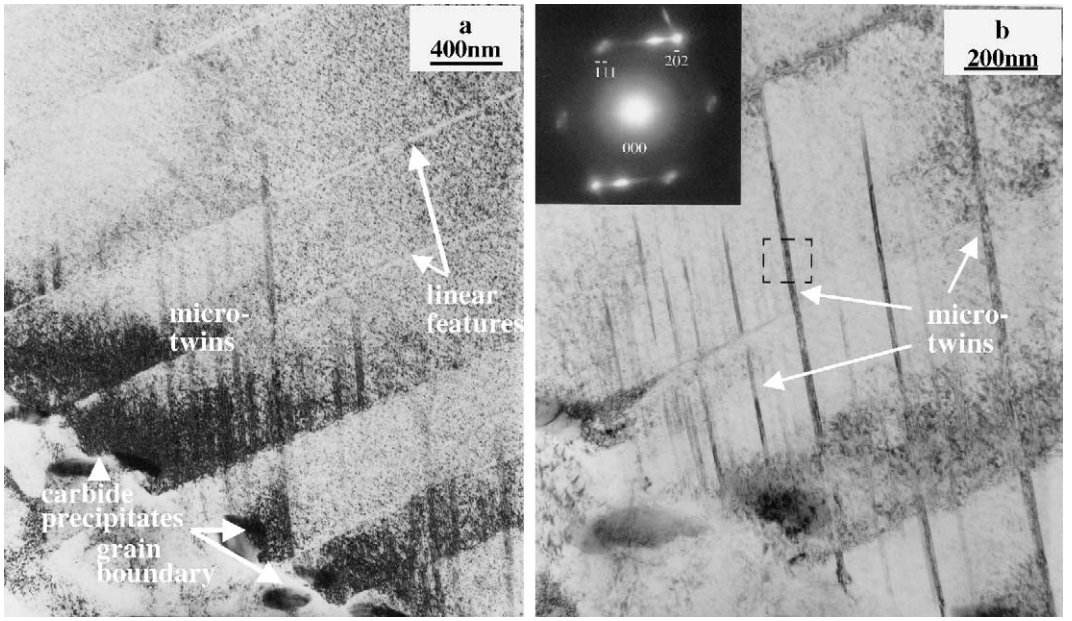

Fig. 12. Low and high magnification images of linear features and microtwins at or near to grain boundary on the [1 1 1] type planes (a). A higher magnification image and the SADP from a microtwin (marked with a square) (b).

planes that have a spacing of about 100 nm, implying that adjacent to the grain boundary significant deformation took place. When viewed with beam direction $B = [1\,0\,1]$, the SADP taken from a microtwin (marked with a square) in a higher magnification image shows the presence of extra diffraction spots around all the variants of the [1 1 1] matrix selection and the [2 0 2] matrix reflections (as marked) (Fig. 12(b)). This confirms the presence of microtwins on all variants of the [1 1 1] planes.

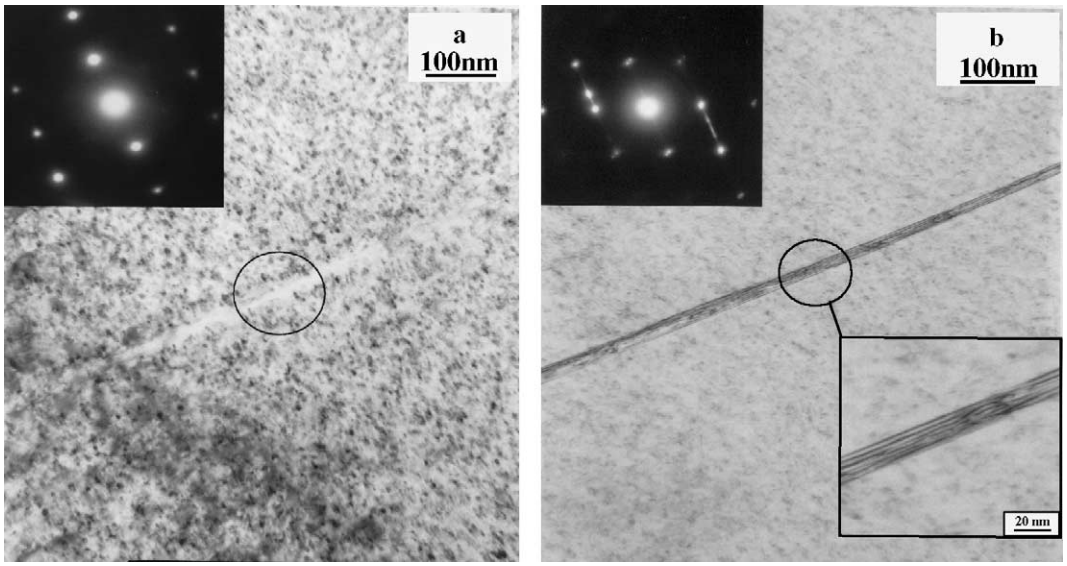

Fig. 13. The linear feature running up to the grain boundary. Imaged with beam direction $B = [1\,1\,2]$, the feature appears as a channel (a). If sample is tilted to beam direction $B = [1\,0\,1]$, the channel walls being in fact made up of twin character (b).

Fig. 13 shows a high magnification linear feature running across the grain up to the grain boundary. Imaged with electron beam direction $B = [1\,1\,2]$, the feature appears as a channel, clear from dislocation loops. The SADP shows no extra twin reflections and thus no evidence of twin reflections (Fig. 13(a)). However, if sample is tilted to beam direction $B = [1\,0\,1]$, it is clear that the channel walls are in fact made up of twin character. The SADP shows the presence of twin reflections (Fig. 13(b)).As there were no microtwins in the regions from which the SADP was taken, the twin reflections indicate that the linear features are actually a deformation twin and not a dislocation channel.

In summary, the character of the linear features was observed to vary depending on the degree of deformation between or within grains. As deformation increased, the linear features changes from dislocation tangles to channels, free from loops. In regions of high deformation, deformation twins replaced the channels.

3.2.2. Specimen thickness center region

Deformation microstructures in the central region of the specimen were found to be dominated by linear features/deformation twins on all variants of the [1 1 1] type planes. The number and spacing of deformation twins varied from region to region, depending on the grain orientation with respect to thin TEM foil sample, especially taken from the necked portion of the specimen. The regions enclosed by the deformation twin boundaries contained radiation induced dislocation loops and grain boundary Cr-carbides ($M_{23}C_6$). It was confirmed with the SADP that both the microtwins and dislocation loops were formed on the [1 1 1] type planes.

Fig. 14 represents variations in TEM microstructures at the thickness center region with distance from the fracture face. In general, fewer linear features/deformation twins have a wider spacing with increasing distance from the fracture face. The number density of microtwins was also significantly less with increasing the distance. There were no regions containing line dislocations at any positions of the gauge section having IG cracks. At a position 8.3 mm from the fracture face, no evidence of microtwins or dislocation lines other than radiation-induced loops were there anymore in the microstructure, although an occasional deformation twinning was observed.

4. Discussion

It has shown that the most significant fractographic evidences characterizing the IG cracking in the surface region of 304 SS irradiated to 1.2×10^{21} n/cm^2 and fractured in 290 °C inert gas were various geometric patterns of linear features/steps with a spacing of the order of 2–3 μm on the IG grain facets. The TEM deformation microstructures typical of the near surface region where numerous IG cracks were present revealed that the linear features/deformation twins and microtwins were predominant, especially at or near grain boundaries. Obviously these features that are originated in a high density of radiation-induced dislocation loops are linked to the processes of the inhomogeneous localized plastic deformation in the 304 SS irradiated to 1.2×10^{21} n/cm^2. On the contrary, those for the material unirradiated and irradiated to 1.1×10^{20} n/cm^2, in which

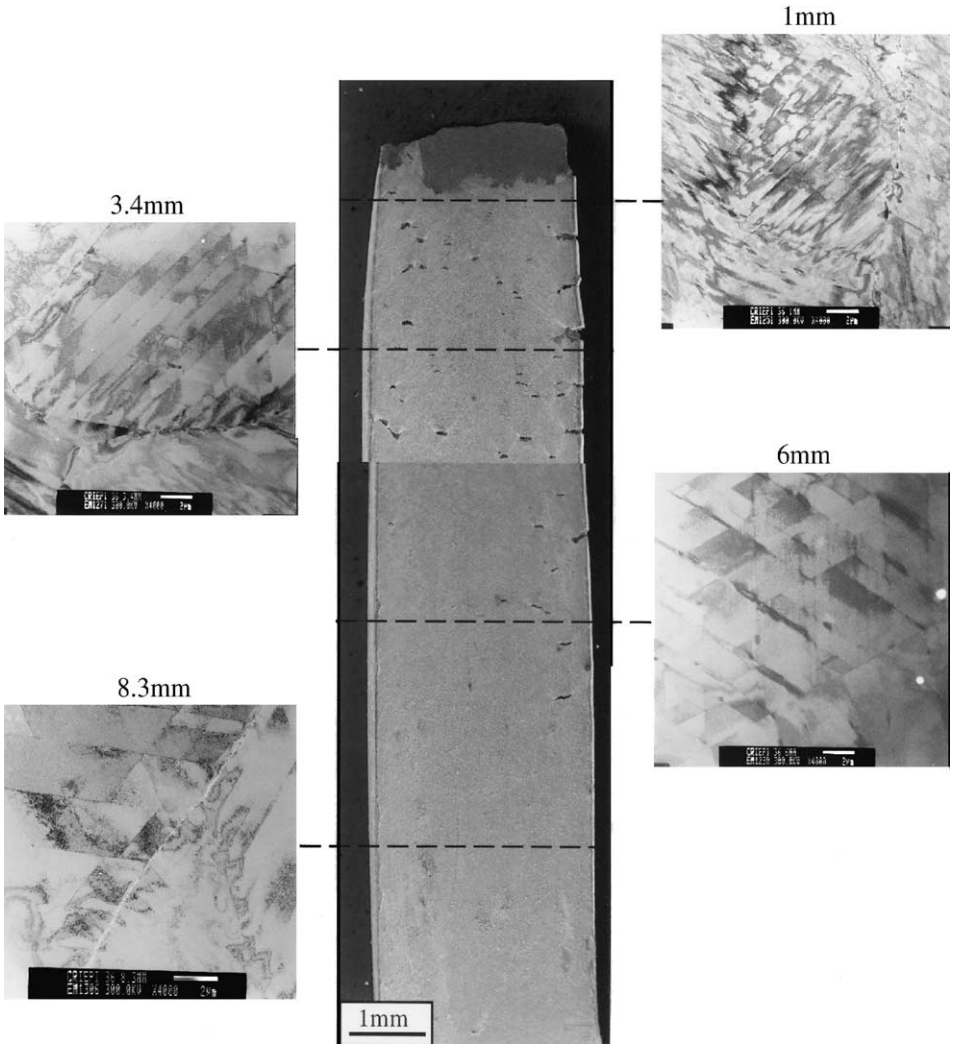

Fig. 14. Variations of TEM microstructures in the thickness center regions with distance from the fracture face.

radiation induced dislocation loops were not readily observed, did not show any distinct inhomogeneous dislocation structures, as represented in Fig. 15. The dislocation cell structures of the unirradiated material ruled the entire deformation to ductile fracture (Fig. 15(a)) and pseudo-linear features of the material irradiated to 1.1×10^{20} n/cm^2 controlled the mechanical performance (Fig. 15(b)).

4.1. Linear features

In general, radiation-hardened materials plastically deform in an inhomogeneous manner due to the formation of cleared channels, in which radiation-produced dislocation loops are swept away, and subsequently slip deformation develops primarily in the narrow channels of the irradiated and deformed materials. Such an inhomogeneous deformation is known to occur in the irradiated metallic material regardless of crystallographic structures. This sort of inhomogeneous plastic deformation localization peculiar to the irradiated metals is designated as dislocation channeling, as noted by Wechsler [13], who described that the term denotes the process by which glide dislocations remove the defect clusters (black spots and dislocation loops observed by TEM) produced by neutron irradiation or quenching, resulting in the formation of cleared channels. Subsequent deformation is enhanced in the channel relative to the radiation-hardened matrix, and coarse, concentrated deformation ensues. This means that the glide dislocation plays a key role on the occurrence of dislocation channeling. In facts dislocation lines are identified usually

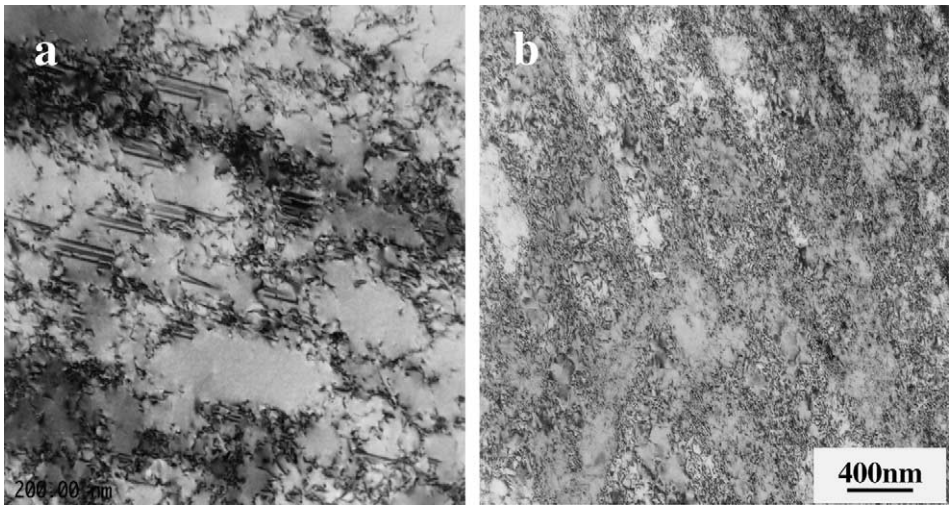

Fig. 15. Typical TEM deformation microstructures: for unirradiated (a) and 1.1×10^{20} n/cm^2 (b).

alongside the wall of channels and dislocation tangles at the intersection of channels. However no knowledge has been gained, except for Bloom [1] as noted previously, whether and how the localized slip deformation results in changing fracture mode from ductile to brittle manner in the irradiated austenitic SSs.

Concerning the plastic deformation of the irradiated austenitic SSs, detailed TEM observations have been made by several workers [3,5,14–16], who studied features of plastic deformation mechanism in neutron and proton irradiated SSs. Hashimoto et al. [3] investigated plastically deformed microstructures by TEM on a 0.76 mm thick flat specimen of the solution annealed J316 SS irradiated to 7 dpa at 330 °C in the ORR reactor and subsequently deformed by SSRT at the same temperature in a vacuum. He showed that twinning was the predominant deformation mode and dislocation channeling as well. Chung et al. [5] also studied TEM deformation microstructure of the solution annealed 304 SS irradiated to about 50 dpa at approximately 370 °C in the EBR-II reactor and tested by SSRT at 289 °C in air and in low electrochemical potential water, insisting that twinning and dislocation channeling were the predominant deformation mechanism in air and in water, respectively. The dislocation channeling, which Hashimoto et al. [3], Chung et al. [5], Bruemmer et al. [14], and Victoria and his co-workers [15,16] insisted to have observed, is not certain because they have not shown any SADP evidence of dislocation channel. Since those workers have not experienced any occurrence of the IG cracking in an environment of no water, they could not directly correlate their TEM microstructures with the IG cracking. Nevertheless it is likely that the deformation twinning and the linear features similar to the dislocation channels are the common mechanism of plastic deformation in the SSs irradiated either with neutron or with proton ion, although their experimental conditions such as material, irradiation method, and SSRT method are significantly different among the individual workers.

In the present work, the TEM examination of the surface region in which IG cracks were present showed only a few dislocation lines and deformation twins in the low deformation microstructure (Figs. 9 and 11), and deformation twins in the high deformation microstructure, which were identified in the high magnification linear features by the SADP (Figs. 12 and 13). Therefore we have termed the inhomogeneous deformation structures of the neutron-irradiated SSs not as slip/steps but as linear features/steps in SEM fractographic observations, and not as dislocation channeling but as linear features/deformation twinning and microtwins in the TEM structures. A high density of radiation induced dislocation loops and a high density of microtwins were also present in the irradiated SSs in which a number of IG cracks were formed. The SADP confirmed that both radiation induced dislocation loops and microtwins were on the [1 1 1] type planes (Figs. 9 and 10). In grains with a high level of deformation, the number of microtwins generally increased at or near the grain boundary (Fig. 12). The resulting microstructures of a large number density of microtwins adjacent to grain boundaries have proved to be in a large level of deformation. In addition, grains with a lower level of deformation, microtwins were generally absent, replaced by microtwin nuclei (Figs. 9–11), although the presence of microtwins and microtwin nuclei make interpretation of the observed features complicated.

In addition to these background features, the main microstructures are the presence of large number of linear features, which apparently played the most

Table 3
A summary of the TEM examinations in the surface region of the specimen irradiated to 1.2×10^{21} n/cm^2 and deformed to fracture

Variant	Deformation levels and regions	Descriptions	Remarks
#1	• Lower deformation grains • Away from and parallel to the grain boundary	Viewed with $B = [1\,0\,1]$, • linear features are made up of dislocation tangles and very fine microtwin nuclei (Fig. 9)	Grain B
#2	• Lower deformation grains • Closer and parallel to the grain boundary	Viewed with $B = [1\,0\,1]$, • linear features are channels of no dislocation loops present • the channel appears to be bounded at the channel wall by microtwin nuclei (Fig. 10)	Grain B
	• Lower deformation grains • Adjacent and parallel to the grain boundary	Viewed with $B - [1\,0\,1]$, • linear features, clear from loops, are a fully developed deformation twin • the channel is bounded with fringes • linear features are of twin character and not dislocation channel (Fig. 11)	
#3	• High deformation grains • Close to the grain boundary	Viewed with $B = [1\,1\,2]$, • linear features appear as channels, clear of dislocations loops • linear features are of twin character • bands of microtwins lying on the [1 1 1]type planes (Fig. 12)	Grain A
	• High deformation grains • Away from the grain boundary	Viewed with $B = [1\,0\,1]$, • linear features are of twin character and not a dislocation channel • linear features are deformation twin (Fig. 13)	

important role on the IG cracking of the irradiated 304 SSs. Although the low magnification linear features are similar to each other, it becomes clear from the high magnification examinations, combined with the SADP, that there are approximately three variants present within the surface regions of the IG cracks in the irradiated material. Table 3 summarizes the TEM observation of the linear features in the surface region where a number of IG cracks were present. The three variants, #1, #2 and #3, of linear features that were identified on the same habit plane of [1 1 1] type appear to depend on either lower or higher level of plastic deformation, and on either away from or near to grain boundaries. Among the three variants of the linear features, variant #1 appears to be formed away from the grain boundary at the lowest level of deformation, which is evidenced by the presence of dislocations running across the grain, with associated microtwin nuclei (Fig. 9). This may be the start of formation of a channel features. As closer and parallel to the grain boundary, variant #2 appears to originate in variants #1, as indicated in Fig. 10. Upon increased deformation, variants #1 and #2 are replaced with variant #3 deformation twins. As the deformation and local stress increases at the grain boundary, the microtwins and microtwin nuclei can be readily nucleated as observed in Fig. 13.

The linear features of the surface layer where IG cracks are present in the irradiated 304 SS in this work are similar to deformation twins observed by Hashimoto et al. and Chung et al. in neutron irradiated SSs and by Bruemmer et al. in proton and heavy ion irradiated SSs and by Victoria et al. in proton and neutron irradiated SSs, although their irradiated samples were of no IG cracks. However, the individual deformation twins cannot be regarded as a key factor for the IG cracking. A high number density and a strong interaction of deformation twins with the grain boundary should result in generating a high number density of microtwins at or near the grain boundary. Further more their TEM observations of dislocation channels and deformation twins are not well characterized by the SADP. In the present work, deformation twins, microtwins and microtwin nuclei were well characterized by the SADP. From the above general observation, therefore, deformation

twinning and microtwins themselves appear to play much more important role on the IG cracking than expected, when their number density is large.

4.2. IG cracking process

It has been generally acknowledged that the macroscopic deformation slip in the fracture surface and microscopic dislocation channeling structures are linked together in fcc, bcc and hcp metals when those materials are irradiated and plastically deformed to fracture. The localized plastic deformation in narrow dislocation channels is recognized to induce an extremely small strain to maximum stress, resulting in an earlier onset of plastic instability in the irradiated materials [13]. In the irradiated 304 SS we correlated the SEM fractographic linear features/steps in the IG facets with the TEM microstructural linear features/deformation twinning and microtwins at or near grain boundaries by examining the surface region where the IG cracks were present. That the reduction in the strain to maximum stress with increasing neutron fluence in irradiated SSs, as shown in Table 2, can also be interpreted in terms of linear features/deformation twinning. However it is not resolved yet why and how both the linear features/deformation twinning and grain boundaries can induce the IG crack initiation in the irradiated SSs, although Bloom [1] interpreted the IG crack initiation of the irradiated austenitic SSs in terms of the interaction between dislocation channels and the grain boundary.

It has become apparent from this work that the deformation twins were nucleated and grew in the linear channel and also a higher number density of microtwins appeared at or near grain boundaries, as observed in Figs. 12 and 13. The predominant deformation twinning and extremely less slip dislocations in the channel are not specific to the surface region where the IG cracks were present in the irradiated 304 SSs, because they are also present in the specimen center region where the IG cracks were absent. We suggest that the predominating linear feature/deformation twinning may be necessary but not sufficient for the IG crack initiation. The higher number density of microtwins is an important evidence of high stress and strain concentrations at or near grain boundaries. In facts, at the regions where IG cracks are absent, no such higher number density of microtwins and linear features/deformation twinning at or near grain boundary were identified. In order for the IG cracking to be able to initiate at the grain boundary, it is required that a higher concentration of stress and strain is generated at the impingement of deformation twins and grain boundaries, and also that the slip deformation systems are unable to be readily activated. The deformation twinning which are confined in the narrow linear channels with less slip deformation would be able to become another source of the higher stress at the grain boundary and the twin boundary. Thus the deformation twins in the linear channels could also act as the cracking paths for channel fracture, as found in Figs. 3(c), 4(b) and (c).

The surface region of the highly irradiated SSs meets the requirements of higher local stress and strain concentrations and less activated deformation systems, because the stress and strain condition in the surface region of the radiation hardened material is in a plain strain stress condition, resulting in severely restricted operations in the deformation systems, in comparison with the interior of the material in a multi-axial stress state during straining up to the plastic instability in the SSRT. In addition the irradiated thermally sensitized 304 SS is known to suffer enrichments of residual impurity elements such as phosphorous and silicon and an alloying element like nickel at grain boundaries due to both thermal sensitization heat treatments and radiation induced segregation. Since the segregation can act as reducing grain boundary cohesion, it would be effective for initiating the IG cracks, although Bloom [1] suggested that the radiation induced segregation at the grain boundaries does not appear responsible for the IG crack initiation. In fact, the grain boundaries in the ductile dimple patterns, obtained in 290 °C inert gas, for the thermally sensitized 304 SSs are clearly visible at the higher fluence but less clearly at the lower fluence and unirradiated condition, as shown in Fig. 16. The role of the grain boundary carbides precipitates on deformation and fracture is still uncertain, since there is no clear evidence for the microtwins to interact strongly with the precipitates at the grain boundary.

Most of all the metallurgical features at or near the grain boundaries are likely to be favorable for the IG fracture of the thermally sensitized 304 SSs irradiated to 1.2×10^{21} n/cm^2, because the occurrence of the IG cracking is a process in which the highly concentrated stress is released at the grain boundaries. Among various radiation produced features, a higher density of linear features/deformation twins is a primarily important factor for causing the IG cracking, because this microstructural features specific to the irradiated SSs appear at a higher fluence of 1.2×10^{21} n/cm^2 but not at a lower fluence of 1.1×10^{20} n/cm^2. Regarding the influence of twining on fracture behavior of fcc metals, an extensive review was made by Lemy [17], who pointed out that the deformation twins can act as a site for crack initiation as well as propagation and the grain boundaries and the twin boundaries can constitute the sites and the paths for the IG and transgranular (TG) cracking at the twin-grain boundary impingement. As seen in Figs. 3(c), 4(b) and (c), fracture along the linear feature or deformation twins was also observed. Therefore the deformation twins in the linear features are likely to result in more readily causing the IG cracks when interacted with the grain boundary and also TG fracture at the deformation twin boundary.

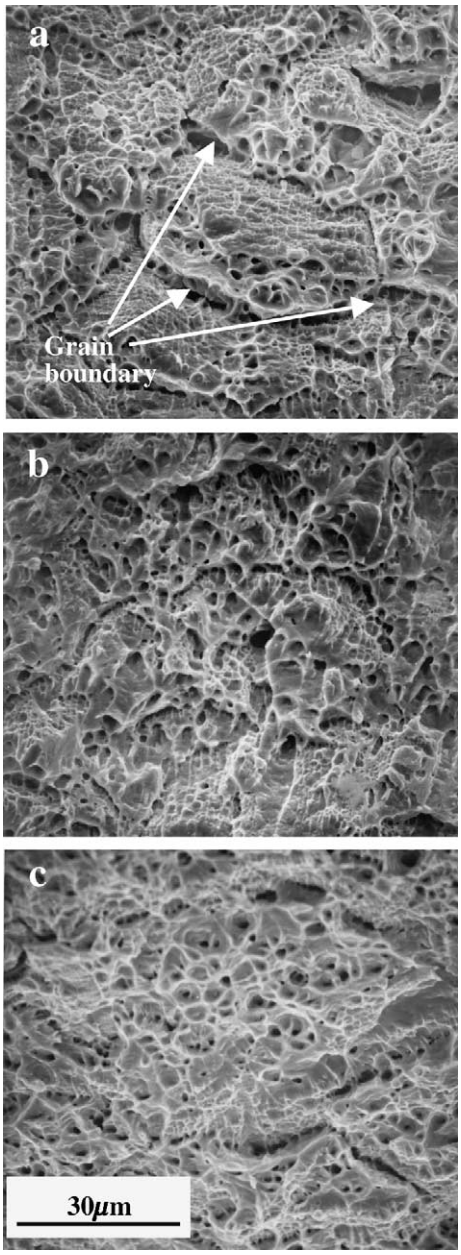

Fig. 16. Examples of grain boundary traces in the ductile dimple pattern in the thermally sensitized 304 SS irradiated and fractured in 290 °C inert gas: for 1.2×10^{21} n/cm^2 (a), 1.1×10^{20} n/cm^2 (b), and unirradiated (c).

It has become apparent from this work that there is a mechanism mechanically causing the IG cracking in the irradiated austenitic SSs even without water environment. From this fact we can deduce that when a higher level of stress and strain concentration which is evidenced by a high number density of microtwins is realized at the grain boundary, the water environment is not absolutely effective for the initiation of IG cracking even if the IG cracks were found in a water environment. It is also a logical thinking to assume that the high number density of deformation twining in the linear feature and the high population of microtwins at or near grain boundaries are more essential for the nucleation and initiation of the IG failure in the highly irradiated SSs. It however should be kept in mind that the knowledge acquired in this study is for the thermally sensitized 304 SSs irradiated to 1.2×10^{21} n/cm^2 and not for the solution annealed and cold-worked SSs. An implication to the IASCC initiation mechanism will therefore be such that the sites of the grain boundary and/or twin boundary, which high stress and strain concentrations acted on due to a strong interaction or the impingement by the deformation twining is hypothesized to be potential sites for the IASCC crack initiation in water environment and the high level of stress and strain concentration is more essential than the water environment for nucleating and initiating the IG cracks in the surface region of the irradiated SSs.

5. Conclusions

Detailed fractographic and microstructural characterizations were made and correlated to each other for the surface region, where a number of IG cracks were present, of the thermally sensitized 304 SSs irradiated to 1.2×10^{21} n/cm^2 and subsequently fractured intergranularly at 290 °C in inert gas by SSRT.

(1) A number of IG cracks were identified in the surface region of the deformed and fractured material. The grain facets in the IG cracks showed various geometric patterns of linear features/steps and also evidences of fracture along the linear features. The TEM microstructures of the surface region revealed a high number density of the linear features/deformation twinning at or near the grain boundaries and also a high population of microtwins at the grain boundaries.

(2) High magnification TEM examinations combined with selected area diffraction analysis identified three variants of linear features present on the [1 1 1] habit plane, depending on a level of plastic deformation and also on either near to or away from the grain boundary. In more deformed grains the number of microtwins appears to increase at the grain boundary whereas in less deformed grains microtwins were absent, replaced by microtwin nuclei, at the grain boundary.

(3) A high number density of microtwins at the grain boundary evidences a high local stress and strain concentration, which may nucleate and initiate IG cracks at the impingement of deformation twins and grain boundaries, although the predominating deformation twinning in the linear features is necessary but not sufficient for the IG cracking. The deformation twin

boundary can also act as fracture path along the linear features. A reduction in the grain boundary cohesion, if any, may be effective for the crack initiation.

(4) A mechanism mechanically causing the IG cracking in non-aqueous environment is present in the highly irradiated austenitic SSs. This means that even if the IG cracks occur in water environment, the water environment itself is not absolutely effective for initiating the IG cracks. In the mechanistic consideration of IASCC initiation, the high stress and strain concentration, evidenced by the high number density of microtwins, is hypothesized to be more essential than the water environment.

Acknowledgements

Authors are grateful to Ms T. Karlsen at IFE, Norway and Professor H. Matsui at Tohoku University, Japan for performing neutron irradiation of the materials at Halden Reactor and at JMTR, respectively.

References

[1] E.E. Bloom, in: N.L. Peterson, S.D. Harkness (Eds.), Radiation Damage in Metal, The American Society for Metals, Ohio, 1975, p. 295.
[2] T. Onchi, K. Hide, M. Mayuzumi, T. Hoshiya, Corrosion 56 (2000) 45.
[3] N. Hashimoto, S.J. Zinkle, A.F. Rowcliffe, J.P. Robertson, S. Jitsukawa, J. Nucl. Mater. 288 (2001) 179.
[4] J. Morisawa, M. Kodama, N. Yokota, K. Nakata, K. Fukuya, S. Shima, K. Asano, J. Nucl. Mater. 294 (2001) 241.
[5] H.M. Chung, R.V. Strain, W.J. Shack, Nucl. Eng. Design. 208 (2001) 22.
[6] P.M. Manahan, R. Kohli, J. Santucci, P. Sipush, Nucl. Eng. Design. 113 (1989) 297.
[7] T. Matsuoka, T. Yonezawa, M. Tomimatsu, M. Mori, H. Myojin, Y. Sasaki, M. Ootani, T.Y. Nagata, JSME Int. J., Ser. A 38 (1995) 515.
[8] G. Furutani, N. Nakajima, T. Konishi, M. Kodama, J. Nucl. Mater. 288 (2001) 179.
[9] A. Jenssen, L.G. Jungberg, in: T. Shoji, T. Shibata (Eds.), Proc. Int. Symp. on Plant Aging and Life Prediction of Corrodible Structures, JSCE and NACE International, Tokyo, Japan, 1996, p. 733.
[10] S.M. Bruemmer, in: Proc. 10th Int. Conference. on Environmental Degradation of Materials in Nuclear Power Systems – Water Reactors, Lake Tahoe Nevada, 5–9 August 2001, NACE International, Houston, TX, 2002.
[11] T. Onchi, K. Hide, M.L. Castano, M. Navas, in: Proc. 10th Int. Conference. on Environmental Degradation of Materials in Nuclear Power Systems – Water Reactors, Lake Tahoe Nevada, 5–9 August 2001, NACE International, Houston, TX, 2002.
[12] M.L. Castano, M. Navas, D. Gomez-Briceno, T. Onchi, K. Hide, in: Proc. 10th Int. Conference. on Environmental Degradation of Materials in Nuclear Power Systems – Water Reactors, Lake Tahoe Nevada, 5–9 August 2001, NACE International, Houston, TX, 2002.
[13] M.S. Wechsler, The Inhomogeneneity of Plastic Deformation, ASM, Ohio, 1973, p. 19.
[14] S.M. Bruemmer, J.I. Cole, J.L. Brimhall, R.D. Carter, G.S. Was, in: Proc. 6th Int. Conference. on Environmental Degradation of Materials in Nuclear Power Systems – Water Reactors, TMS, Warrendale, PA, 1993, p. 537.
[15] M. Victoria, N. Baluc, C. Bailat, Y. Dai, M.I. Luppo, R. Schaublin, B.N. Singh, J. Nucl. Mater. 276 (2000) 114.
[16] C. Bailat, F. Groschel, M. Victoria, J. Nucl. Mater. 276 (2000) 283.
[17] L. Lemy, Metal. Trans. A 12 (1981) 387.